Progress In Electromagnetics Research B, Vol. 60, 227–239, 2014

Efficient Isolation between Electrically Small Metamaterial-Inspired Monopole Antennas

Nektarios K. Bourgis* **and Traianos V. Yioultsis**

Abstract—In this paper, a new electrically small metamaterial-inspired monopole antenna is presented. It consists of a simple square-shaped coplanar waveguide (CPW-fed) monopole with an embedded complementary split ring resonator (CSRR). It operates at three distinct frequency ranges around 2.45, 4.2, and 5.8 GHz, with low return loss and uniform radiation patterns, making it a perfect candidate for modern wireless applications. Furthermore, using this as a primary unit to construct two different 2×2 MIMO configurations, we achieve systematic minimization of mutual coupling, using additional single negative (SNG) metamaterial-inspired resonators. Mutual coupling is reduced by as much as 27 dB at the frequency of interest. Simulated and measured results of all antennas are in good agreement.

1. INTRODUCTION

Metamaterials (MTMs) are a modern class of composite, effectively homogeneous structures, exhibiting unusual physical properties not found in nature. They are formed by periodically arranged subwavelength unit cells, exhibiting negative effective electrical permittivity (ϵ_{eff}), magnetic permeability (μ_{eff}), or both, simultaneously [1–3]. Their unique properties stem from the unit cell structure, rather than the constituent materials. Therefore, their response to an electromagnetic wave can be predicted by their unit cell structure. Different parameter retrieval methods have been developed to predict the values of the effective permittivity and permeability, based on S-parameters with the metamaterial being treated as a homogeneous medium, due to the subwavelength size of its unit cell [4–6]. This fact has been the basis for a variety of different applications since their first experimental demonstration [3].

Recently, there has been a steady growth of interest in metamaterial-inspired antennas research and design [7–18]. These antennas provide enhanced performance characteristics by utilizing specific single negative, MTM-based subwavelength resonators, as inclusions, near the radiating element. Although these inclusions can not be considered as metamaterials in the strict sense, they inherit the characteristic properties of metamaterials. One popular MTM-based resonator is the complementary split ring resonator (CSRR) [19], which is the dual screen of the well-known split ring resonator (SRR) [2]. The CSRR is based on Babinet's principle and duality concept and it exhibits negative permittivity over a specified frequency [20]. Its electromagnetic behavior presents several advantages over its dual counterpart. One of the main advantages of using the CSRR instead of the SRR in antenna technology is its easy integration to planar antennas as an embedded element to ground planes or radiating elements, instead of parasitic ones [21]. In addition, using CPW-fed monopoles, the design can be solely uniplanar, resulting in compact or even electrically small antennas.

The advent of new wireless communications standards such as WiFi and WiMAX requires efficient, multiband and miniaturized antennas for faster data transfers [22]. The aforementioned key performance factors can be delivered by carefully designed metamaterial-inspired antennas. Moreover, multiple-input

Received 13 May 2014, Accepted 4 August 2014, Scheduled 10 August 2014

* Corresponding author: Nektarios K. Bourgis (nbourgis@auth.gr).

The authors are with the Department of Electrical and Computer Engineering, Aristotle University of Thessaloniki, Thessaloniki 54124, Greece.

multiple-output (MIMO) antenna systems with increased channel capacity and substantially reduced multipath fading must be realized [23]. These systems consist of closely packed antenna elements. A key factor for their satisfactory performance is maximizing isolation or effectively reducing the unwanted mutual electromagnetic coupling between radiating elements, which degrades the performance of MIMO systems [24, 25]. Many approaches have been proposed for this purpose, including electromagnetic bandgap structures [26, 27], or metamaterials [28, 29], polarization diversity [30, 31], radiation pattern diversity [32] and other techniques. In our study, mutual coupling reduction is achieved efficiently with SNG metamaterial-inspired inclusions placed in specific areas between the radiating elements, blocking the propagation of electromagnetic waves from one element to another [33–36].

In this paper, we present a new simple uniplanar electrically small CSSR-based antenna, designed for WiFi applications at 2.45/5.8 GHz. The idea of an embedded metamaterial-inspired inclusion to minimize the size of a conventional monopole antenna is applied. The resulting system exhibits three distinct operational frequency bands and behaves in terms of radiation characteristics similar to the conventional monopole, performing omnidirectional coverage. In the next step, the electrically small antenna size is evaluated in terms of its quality factor Q [37–39]. Fabrication of the overall antenna system can be realized with simple standard techniques for low-cost mass production.

Then, we use this antenna as a basis to design MIMO antennas. In particular, two separate configurations with different arrangements of the radiating elements are examined. The use of SNG resonators to reduce mutual coupling at 2.45 GHz and enhanced system performance is reviewed. Standard capacitively loaded-loop (CLL) resonators [40–42] and wire strips [1] are used to systematically enhance isolation between radiating elements. Performance is assessed via the envelope correlation coefficient ρ_e [43]. In addition to simulations, measurements of all antennas have been carried out (using an Anritsu 37397D Lightning network analyzer) and are presented in the following sections.

2. BASIC ANTENNA DESIGN

The uniplanar antenna structure considered in this work is depicted in Figure 1(a), and it is designed on a low-cost 1.6 mm thick FR-4 dielectric substrate with relative permittivity $\epsilon_r = 4.4$, loss tangent $\tan\delta = 0.02$ and a 30 µm thick copper cladding. The CSRR element is hosted in a square patch

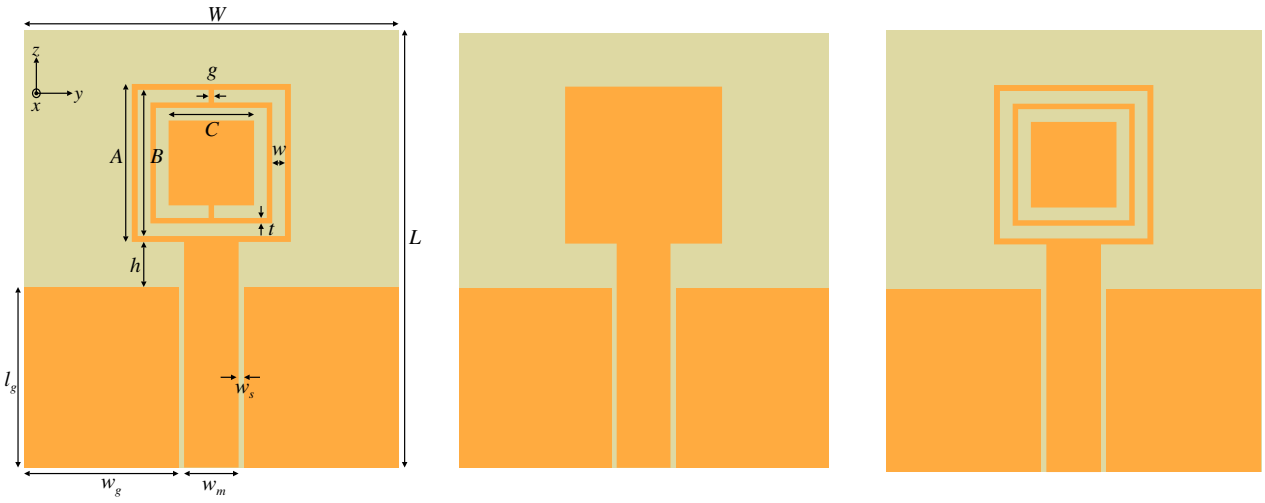

Figure 1. (a) Geometric parameters of the CSRR antenna structure: substrate width $W = 20.6$ mm, substrate length $L = 24.25$ mm, ground width $w_g = 8.5$ mm, ground length $l_g = 10$ mm, line feed width $w_m = 3$ mm, $w_s = 0.3$ mm, $h = 2.5$ mm, patch length $A = 8.75$ mm, $B = 8.1$ mm, $C = 4.7$ mm, aperture width $w = 0.7$ mm, closure width $g = 0.3$ mm, $t = 0.3$ mm. (b) Basic monopole antenna radiation element. (c) Open complementary split ring resonator (OCSRR) version of (a).

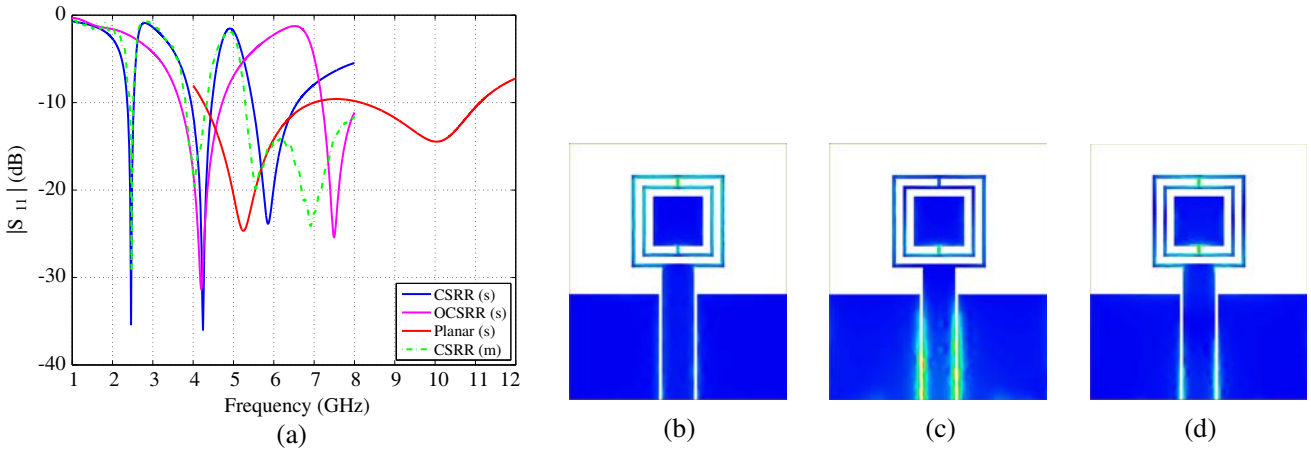

Figure 2. (a) Simulated and measured reflection coefficient of the proposed CSRR antenna. Simulated reflection coefficients of the conventional planar monopole and the OCSRR antenna are also plotted. (b), (c) and (d) Magnitude of surface current density J_{surf}, on the surface of the substrate, at 2.449, 4.244, and 5.858 GHz, respectively. Red areas represent higher values of J_{surf} than blue areas.

monopole element shown in Figure 1(b), with proper size to accommodate the embedded CSRR. To achieve uniplanarity and compactness the antenna feed is a 50 Ω impedance CPW line.

The initial dimensions of the CSRR needed to achieve resonance in the vicinity of 2.45 GHz were estimated by the simulation of its complementary SRR in [15], using a finite element based code [44]. The CSRR and its dual counterpart, i.e., the SRR, are expected to have resonances at frequencies that are close but not exactly the same, due to finite copper thickness and losses [20]. In practice, the resonance of the CSRR appears higher in frequency than the corresponding dual SRR resonance frequency [20]. This means that the CSRR dimensions must be increased to achieve the same resonance frequency as a corresponding SRR. The final dimensions of the overall antenna system are denoted in the caption of Figure 1(a). The corresponding size of the CSRR element is 8.75 mm $\times$ 8.75 mm (merely $\lambda/14 \times \lambda/14$) and the overall antenna size, including the substrate, is 20.6 mm $\times$ 24.25 mm ($\lambda/6 \times \lambda/5$ at 2.45 GHz). It operates at three resonance frequencies, namely at 2.449, 4.244, and 5.858 GHz, respectively, as shown in Figure 2(a) (solid blue line). The corresponding bandwidths at each resonance band are 158 MHz (2.357–2.515 GHz), 515 MHz (3.949–4.464 GHz) and 1.11 GHz (5.471–6.587 GHz), covering adequately the lower and upper designated WiFi frequency bands. The simulated radiation efficiencies at each resonance frequency are 0.7962, 0.8803 and 0.8861, respectively. The measured reflection coefficient of the CSRR antenna is also plotted in Figure 2(a) (dash-dot green line) and the results are in good agreement with the simulated ones.

To further investigate the role of the CSRR element in the antenna frequency characteristics, we implemented it in a way similar to [45], a minor modification of the original antenna with the closures of the CSRR being removed. This open complementary split ring (OCSRR) antenna is shown in Figure 1(c). As it can be seen in Figure 2(a), both the planar monopole and the OCSRR antennas do not exhibit any resonance at 2.45 GHz. Therefore, it can be verified that the lower band response is solely due to the embedded CSRR element. In addition, to identify the frequency function of the CSRR element at each resonance, we simulated the surface current density, J_{surf}. As it can be seen in Figure 2(b), at the first resonance frequency of 2.449 GHz, the current is higher at the top closure. This, in effect, activates the outer bigger CSRR rings. At 4.244 GHz, in Figure 2(c), the current concentrates at the lower closure, activating the inner smaller rings. Finally, at 5.858 GHz, in Figure 2(d), both closures have high concentration of current, leading the whole structure of the antenna to radiate. This radiation is due to the size and shape of the patch hosting the CSRR element. Furthermore, to assess the electrical size of the proposed CSRR antenna, the antenna is considered to be fully enclosed to its Chu sphere [8, 46, 47]. Therefore, the minimum radius a for our antenna (including the ground conductors and the main monopole radiator) is approximately 13.4 mm. A criterion for an electrically small antenna (ESA) is that $k_0 a < 1$ [46], where k_0 is the free space wave number. Our antenna has

an electrical radius of $k_0a \approx 0.688$ or an equivalent overall size of 0.22λ at 2.449 GHz. Nevertheless, fundamental limitations apply between the dimensions of an antenna and its minimum quality factor, commonly known as Chu limit, Q_{Chu}, which is approximately given by [48]:

$$Q_{Chu} = \frac{1 + 2\,(k_0a)^2}{(k_0a)^3\left[1 + (k_0a)^2\right]} \tag{1}$$

It must be stressed that (1) gives the value of Q_{Chu} for the case of an ideal lossless antenna. In our case, the efficiency of our proposed CSRR antenna, as mentioned before, is $\eta = 0.7962$ at 2.449 GHz. Therefore, for our non-ideal lossy antenna, $Q_{Chu_{lossy}} = \eta Q_{Chu}$. The quality factor of the CSRR antenna Q is estimated by the -10 dB fractional bandwidth $FBW_{-10\,\mathrm{dB}}$ of the first resonance [37].

$$Q = \frac{1}{\sqrt{2}FBW_{-10\,\mathrm{dB}}} \tag{2}$$

The ratio $Q/Q_{Chu_{lossy}}$ is equal to 3.39 for our proposed antenna, which indicates that the antenna is sufficiently close to the theoretical limit, even though the antenna is entirely planar and does not exploit the whole volume of the hypothetical sphere. All the corresponding calculated parameters at the first resonance of the antenna, where it exhibits the characteristics of an ESA, are shown in Table 1.

Table 1. Simulated CSRR antenna basic parameters.

Resonance Band	f_0	BW	$FBW_{-10\,\mathrm{dB}}$	k_0a	Q	η	$Q_{Chu_{lossy}}$	$Q/Q_{Chu_{lossy}}$
2.357–2.515 GHz	2.449 GHz	158 MHz	6.45%	0.688	10.96	0.7962	3.24	3.39

Finally, the simulated far-field radiation gain patterns of the CSRR antenna are shown in Figure 3. It is obvious from Figure 3(a) that the embedded CSRR element introduces an additional resonance at 2.449 GHz, having a significant E-plane radiation, apart from the resonance at 5.858 GHz, where the CSRR antenna behaves almost identically as the conventional patch monopole. In addition, in the H-plane of Figure 3(c), although radiation patterns at different frequencies are not directly comparable, we can clearly notice that the CSRR antenna at the first resonance has more omnidirectional characteristics than that of the planar monopole, since the first one is almost uniform, whereas the latter one exhibits a variation of about 2 dB. Moreover, the radiation pattern of the CSRR at the third resonance in the H-plane is again identical to the corresponding radiation pattern at its first resonance. This is again an evidence that the third resonance of the CSRR is attributed to the shape and size of the patch host and not due to the CSRR element. Finally, the E- and H-plane cross-pol patterns are reported in Figure 3(b) and Figure 3(d), respectively, indicating very low levels of the cross-polarized components, especially for the lowest resonance.

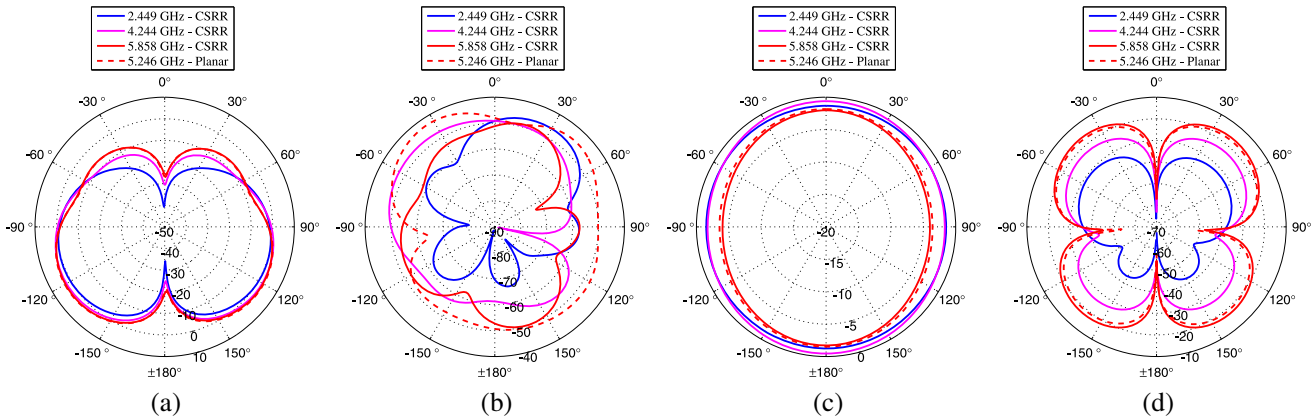

Figure 3. Simulated far-field gain patterns of the CSRR antenna at its resonances and at the first resonance frequency of the simple planar monopole. (a) E-plane co-pol ($\phi = 0°$ and $\phi = 180°$). (b) E-plane cross-pol ($\phi = 0°$ and $\phi = 180°$). (c) H-plane co-pol ($\theta = 90°$). (d) H-plane cross-pol ($\theta = 90°$).

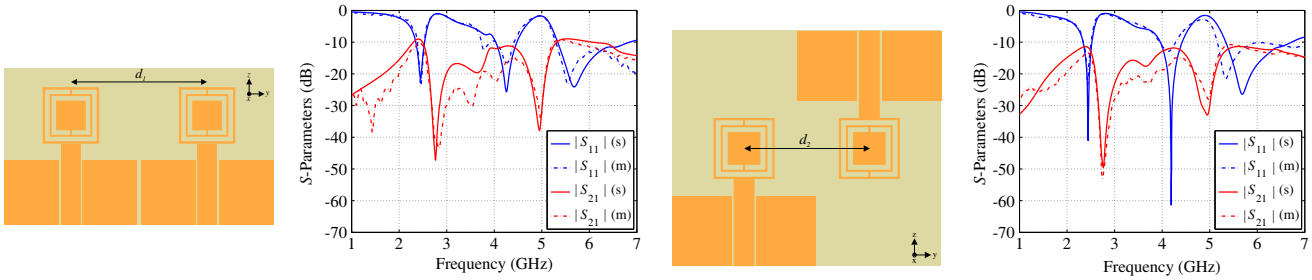

Figure 4. (a) MIMO configuration with adjacent CSRR antenna elements. Dimension $B = 8\,\text{mm}$ (from Figure 1(a)). (b) Simulated and measured S-parameters versus frequency of (a). (c) MIMO configuration with CSRR antenna elements in opposite sides of the substrate. Dimension $B = 8.1\,\text{mm}$ (from Figure 1(a)). (d) Simulated and measured S-parameters versus frequency of (c).

3. MIMO ANTENNAS IMPLEMENTATION AND MUTUAL COUPLING REDUCTION

The proposed CSRR antenna has been used as a basic component for two different compact 2×2 MIMO configurations. The first configuration, shown in Figure 4(a), contains two adjacent CSRR antennas with a fixed distance between the center of the CSRR elements of $d_1 = 21.1\,\text{mm}$. The second one, shown in Figure 4(c), contains two CSRR antennas in opposite sides, in order to reduce their inter-elemental distance to $d_2 = 17.95\,\text{mm}$. The distance between the closest edges of the two CSRR elements are 12.35 mm ($\lambda/10$) and 9.2 mm ($\lambda/13$), at 2.45 GHz, respectively. This characterizes the antenna elements as closely spaced. The choice of the distance between the elements in both cases was made with respect to their marginal performance in terms of mutual coupling ($|S_{21}|$ close to $-10\,\text{dB}$). The dimensions of the dielectric board in the first case are $41.7\,\text{mm} \times 24.25\,\text{mm}$, whereas in the second case are $38.55\,\text{mm} \times 33.75\,\text{mm}$. Therefore, the overall MIMO antennas are considered to be highly compact.

The simulated and measured S-parameters vs. frequency for the two initial configurations are given in Figure 4(b) and Figure 4(d), respectively. The first configuration (Figure 4(b)) has the three resonance bands of 2.350–2.534 GHz (184 MHz bandwidth), 4.030–4.475 GHz (445 MHz bandwidth) and 5.334–6.848 GHz (1.514 GHz bandwidth), with central frequencies at 2.45, 4.256, and 5.68 GHz, respectively. The simulation results of the second configuration (Figure 4(d)) show resonances at 2.444 GHz (2.339–2.552 GHz), 4.191 GHz (3.961–4.421 GHz) and 5.684 GHz (5.339–6.724 GHz). Both MIMO structures offer highly satisfactory bandwidths for WiFi applications, exceeding protocol specifications. The measured results are also shown in the corresponding figures and are in very good agreement with the simulated ones. The mutual coupling between the CSRR antenna elements represented by the transmission coefficient, $|S_{21}|$ reveals that both systems suffer from correlation due to coupling.

Moreover, to further investigate the paths of mutual coupling between the antenna elements in each MIMO antenna configuration, the electric and magnetic field magnitudes are calculated on the surface of the dielectric substrate as shown in Figure 5. It is evident that in both cases, when one radiating element is active while the other is matched to a $50\,\Omega$ termination impedance, most of the radiation power is coupled through the space between the antenna elements and between ground conductors. It is therefore imperative to reduce coupling by use of structures that block or divert this radiation propagation in these specific areas. The design of the MTM-based resonators needed and the systematic approach to deal with the problem of coupling is described in the following sections.

3.1. Design of Resonators

Several types of single negative metamaterial resonators have been proposed and used for mutual coupling reduction between antenna elements in other works. All of them are represented by an LC equivalent resonant circuit. To retain simplicity as our design goal, we propose a double capacitive-

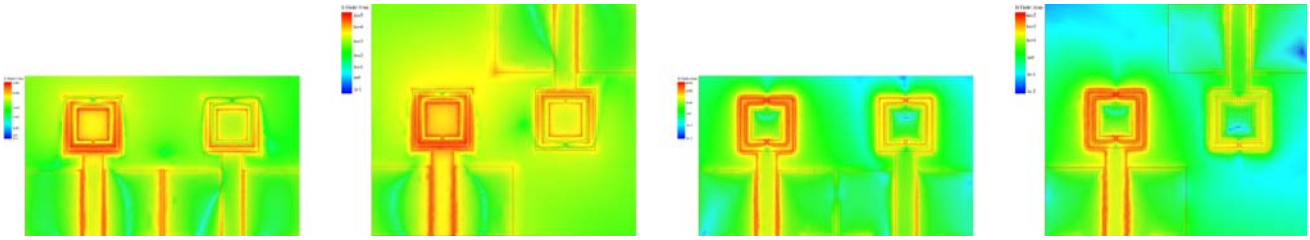

(a) (b) (c) (d)

Figure 5. (a) Electric field magnitude on the surface of the substrate of the MIMO configuration shown in Figure 4(a). (b) Electric field magnitude on the surface of the substrate of the MIMO configuration shown in Figure 4(c). (c) Magnetic field magnitude on the surface of the substrate of the MIMO configuration shown in Figure 4(a). (d) Magnetic field magnitude on the surface of the substrate of MIMO configuration shown in Figure 4(c). The fields are calculated at the central frequency of each antenna's first resonance band. Left port is excited in all cases.

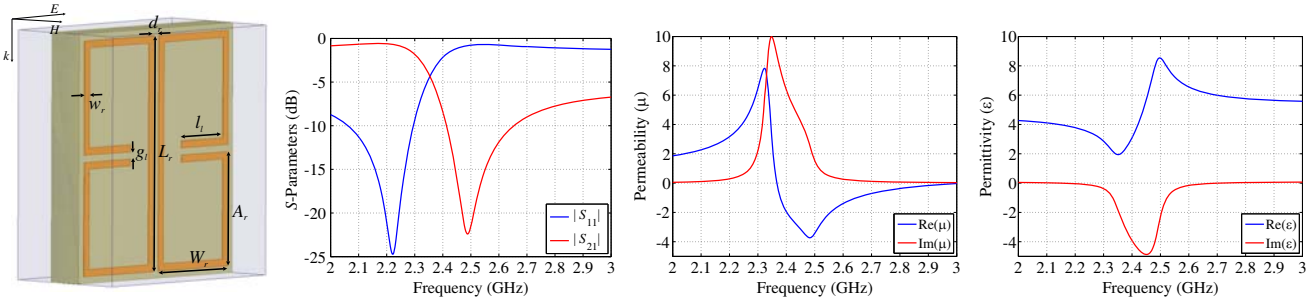

(a) (b) (c) (d)

Figure 6. (a) Geometric parameters of the CLL unit cell: $L_r = 10\,\text{mm}$, $W_r = 4.2\,\text{mm}$, $A_r = 4.85\,\text{mm}$, $l_l = 2.5\,\text{mm}$, $w_r = 0.3\,\text{mm}$, $d_r = 0.3\,\text{mm}$ and $g_l = 0.3\,\text{mm}$. The FR-4 substrate has dimensions of $9.3\,\text{mm} \times 10.6\,\text{mm}$ and a thickness of $1.6\,\text{mm}$. (b) Simulated CLL S-parameters versus frequency. (c) Retrieved real and imaginary parts of complex permeability versus frequency. (d) Retrieved real and imaginary parts of complex permittivity versus frequency.

loaded loop (CLL), shown in Figure 6(a). The CLL element is generally used as a μ-negative (MNG) structure, meaning that when used as unit cell in a periodic array, under the proper polarization of an incoming electromagnetic wave, it exhibits a narrow frequency band around its magnetic response frequency, where the effective permeability is negative. The double CLL metamaterial resonator offers the advantage of symmetry and easy control over scaling its magnetic response frequency, through careful choice of its geometric parameters. In particular, the size of the rectangular rings controls the inductance, while its capacitance is controlled by the various gap sizes. Consequently, it is easy to use fixed values for a set of its geometric parameters to conform its inductance, while appropriately adjusting the value of its capacitance by fine tuning just the one critical dimension l_l (Figure 6(a)). We stress the fact that the CLL resonator is a particularly useful and interesting alternative, compared to other simpler unit cell structures of single negative metamaterials, since it can offer both tunability and particularly small transmission values, along with negative permeability for a wide frequency range, as it will be demonstrated next. In addition, the CLL resonator is expected to provide a pronounced magnetic resonance, compared to other well-known structures like the simple cut-wire plasma, due to its loop structure, while it is uniplanar and clearly provides more parametric variation capabilities. In general, plasma-based structures may need to be designed with a particularly high plasma frequency to ensure an adequate transmission reduction, with the use of only a few unit cells. Nevertheless, the simple wire structure will be exploited as a supplement in various cases, to further improve antenna performance.

The CLL resonator has been designed to block wave propagation on the substrate and the area

between radiating elements, at 2.45 GHz. To retain metamaterial properties at the sample size, its dimensions were chosen to be of subwavelength scale (8.9 mm ($\lambda/13$) $\times$10 mm ($\lambda/12$)). The CLL unit cell was simulated independently using a finite element-based code with appropriate periodic boundary conditions. In our case, perfect electric conductor (PEC) boundary conditions were imposed at the faces of the unit cell perpendicular to the CLL plane, whereas absorbing boundary conditions (ABC) were imposed to the faces parallel to the CLL plane to account for the 2D configuration, in the form of a metasurface. Usual port impedance boundary conditions have been appointed on its top and bottom sides, to simulate the propagation of the electromagnetic wave shown also in Figure 6(a). The calculated reflection and transmission coefficients are presented in Figure 6(b). It is obvious that the transmission coefficient $|S_{21}|$ possesses a minimum very close to the vicinity of the target frequency of 2.45 GHz. Then, the results of the S-parameters of the CLL unit cell can be used to extract the permeability, using a standard parameter retrieval technique. The calculated real and imaginary parts of the complex permeability are shown in Figure 6(c), whereas the corresponding graphs of complex permittivity are shown in Figure 6(d). The unit cell exhibits a negative permeability frequency band from 2.372 GHz and extending up to 3 GHz, where it prohibits wave propagation of the appropriate polarization, based on the physics of evanescent waves and not a loss mechanism. It is essential to note that this procedure is only an indicative approximation to help us trace the function of a single metamaterial-insiped resonator, once the aforementioned process is applicable to real periodic metamaterial media and not to individual cells. We also stress that since the CLL unit cell provides a wide frequency band of negative μ, a particularly appealing consequence is that this metamaterial can be exploited close to a frequency (in this case close to 2.5 GHz), where $\mathrm{Im}(\mu)$ is expected to be particularly low and far below its maximum, as it is evident in Figure 6(c). Nevertheless, negative μ introduces losses and, therefore, the proposed technique relies on mitigating coupling by adding some losses to the system.

To further intercept the action of the mutual coupling at the areas between the ground conductors of the MIMO antenna elements, we chose to select the known thin strips resonators shown at the inset of Figure 7(a). The significant amount of coupling presented at these areas dictates the use of a broadband negative permittivity medium, prohibiting electromagnetic wave propagation in a greater span than the CLL element. Its advantages are that it is simple in fabrication and it can be directly embedded in the ground conductors without any additional area usage. The simulated S-parameters for the thin strip are shown in Figure 7(a). Similarly, the extracted values of real and imaginary parts of the complex permittivity are shown in Figure 7(b). It is evident that the real part of the complex permittivity is negative for the whole span of the first resonance band of the MIMO antenna systems, revealing that the thin strip can function satisfactory as a metamaterial inspired structure to enhance isolation.

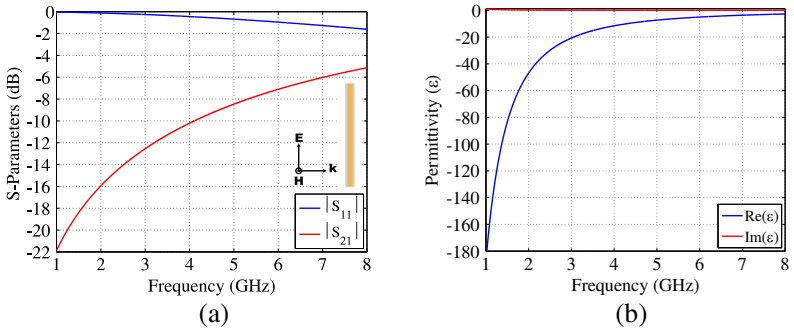

Figure 7. (a) Strip unit cell (inset). Simulated S-parameters versus frequency of the strip unit cell. The strip is 10 mm long and 0.3 mm wide. The FR-4 substrate has dimensions of 0.6 mm $\times$ 10 mm. (b) Retrieved real and imaginary parts of complex permittivity versus frequency.

3.2. Adjacent MIMO CSRR Antennas

The MIMO antenna in Figure 4(a) has been modified with an inclusion of a CLL resonator between its radiating elements. The modified MIMO system is shown in Figure 8(a). The dimensions of the CLL resonator are the same as the unit cell in Figure 6(a). To achieve resonance in the vicinity of 2.45 GHz

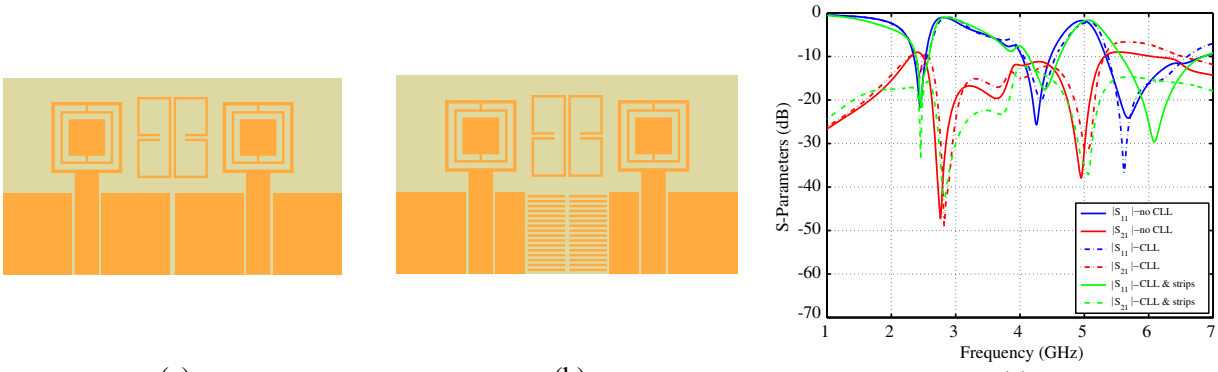

(a) (b) (c)

Figure 8. (a) MIMO antenna with CLL resonator. (b) MIMO antenna with CLL resonator and ground strips. (c) Simulated S-parameters versus frequency.

we slightly tuned the dimension B (from Figure 1(a)) of the CSRR antennas to 7.9 mm. All other dimensions remain the same except C that is now equal to 4.5 mm. The simulated S-parameter results shown in Figure 8(c), reveal that the first resonance band extends from 2.384–2.565 GHz with a center frequency of 2.451 GHz. The mutual coupling $|S_{21}|$, at the center frequency, has been further minimized from −9.26 to −14.79 dB. Therefore, this MIMO configuration operates well in the first resonance band with a bandwidth of 181 MHz. The fact that the CLL resonator was designed to block mutual coupling at the vicinity of 2.45 GHz is evident from the fact that the other two resonant bands of the antenna do not experience any enhancement in isolation.

Figure 8(b) shows a further modification of the original MIMO configuration. Since it has been verified that there is a considerable energy flow in the gap between adjacent ground conductors (Figure 5(a)), further suppression of coupling can be achieved using a proper metamaterial structure in this case as well. In particular, the Poynting vector is shown to have a strong component parallel to the gap (y-axis in Figure 4), while the electric field is directed across the gap. Therefore, a part of the ground structure is replaced by horizontal thin strips, operating in an epsilon-negative metamaterial fashion, as indicated in Figure 7. The strips have a length of 4.6 mm and a width of 0.3 mm, with a 0.3 mm gap between them. The CSRR antennas have the same dimensions as before, with the CLL resonator having $l_l = 2.4$ mm. The simulated S-parameters results show a central frequency of the first resonance band at 2.457 GHz, with a further enhancement of isolation from −14.79 dB to −33.33 dB. The first resonance band extends from 2.389 GHz to 2.58 GHz, with a total bandwidth of 191 MHz.

To evaluate the performance of the 2×2 MIMO antenna configuration, we calculated the envelope correlation coefficient ρ_e given in terms of the S-parameters by:

$$\rho_e = \frac{\left|S_{11}^* S_{12} + S_{21}^* S_{22}\right|^2}{\left(1 - \left(|S_{11}|^2 + |S_{21}|^2\right)\right)\left(1 - \left(|S_{22}|^2 + |S_{12}|^2\right)\right)} \tag{3}$$

For satisfactory performance the envelope correlation coefficient must be lower than 0.5, but in practice, it should be as low as possible. We note that this expression is valid when the radiation efficiency approaches 100%. Therefore, it serves here only as an indicative assessment of mutual coupling reduction. Using (3), the calculated values of ρ_e for all cases of the MIMO antenna configuration with adjacent radiating elements are plotted in Figure 9(a). It is evident that ρ_e progressively goes to lower values as we use the CLL and the thin wire strips. It is approximately zero close to 2.45 GHz for the MIMO antenna with the CLL resonator and the thin strips, demonstrating full decoupling.

Finally, a comparison of the simulated and measured results, for the different cases presented in this section, is shown in Figure 10(a) and Figure 10(c). For the case of the MIMO antenna with the CLL resonator and thin strips, a highly satisfactory value of −26 dB for the mutual coupling was measured at 2.457 GHz. Figure 11(a) also shows the H-plane far-field co-pol radiation pattern for the first resonance, for all different cases of the MIMO configuration. In all MIMO antenna cases, the omnidirectional radiation characteristics are largely retained, whereas some small variations can

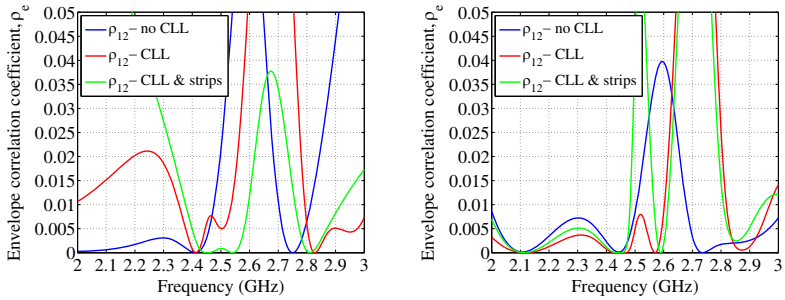

Figure 9. (a) Computed envelope correlation coefficient ρ_e versus frequency for the various cases of the MIMO antenna configuration with adjacent elements. (b) Computed envelope correlation coefficient ρ_e versus frequency for the various cases of the MIMO antenna configuration with opposite elements.

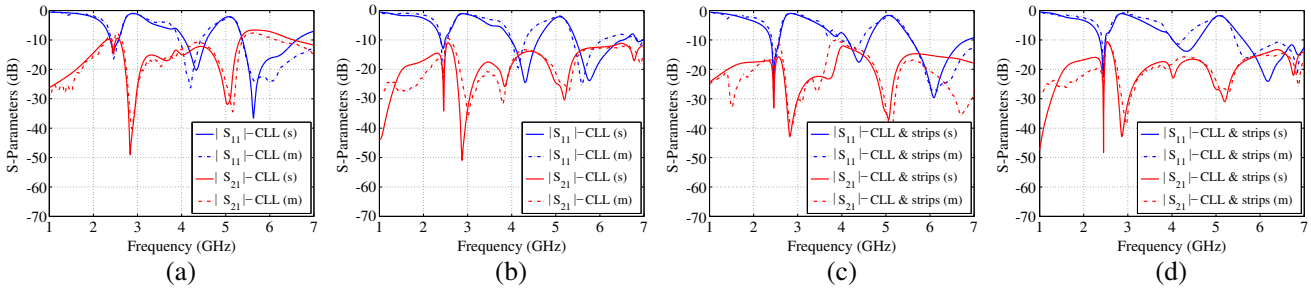

Figure 10. (a), (c) Simulated and measured S-parameters versus frequency for the MIMO antenna with adjacent elements for the cases of Figure 8(a) and Figure 8(b), respectively. (b), (d) Simulated and measured S-parameters versus frequency for the MIMO antenna with opposite elements for the cases of Figure 12(a) and Figure 12(b), respectively.

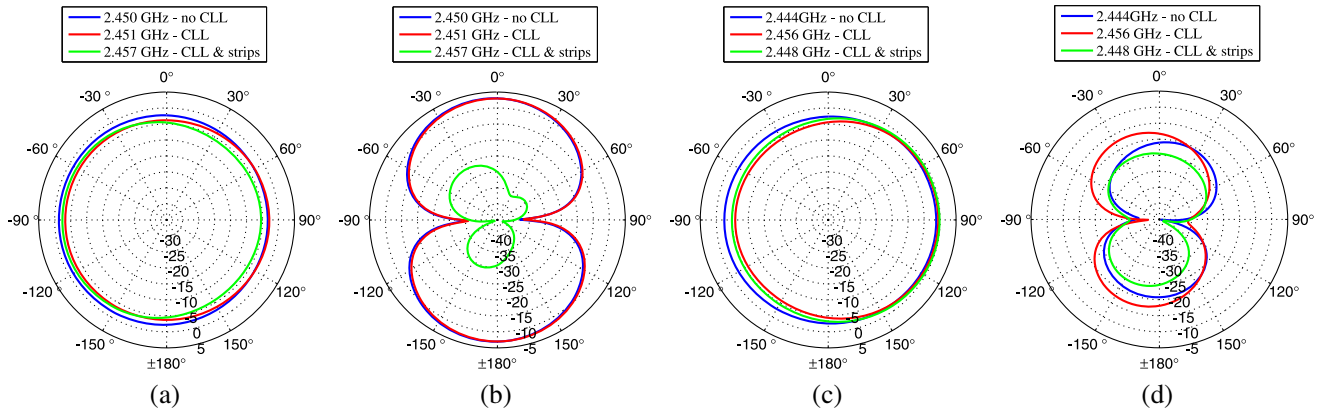

Figure 11. (a) H-plane co-pol ($\theta = 90°$) simulated far-field gain patterns of various cases of the MIMO antenna configuration with adjacent elements at their first resonance band center frequencies. (b) H-plane cross-pol ($\theta = 90°$) simulated far-field gain patterns of various cases of the MIMO antenna configuration with adjacent elements at their first resonance band center frequencies. (c) H-plane co-pol ($\theta = 90°$) simulated far-field gain patterns of various cases of the MIMO antenna configuration with opposite elements at their first resonance band center frequencies. (d) H-plane cross-pol ($\theta = 90°$) simulated far-field gain patterns of various cases of the MIMO antenna configuration with opposite elements at their first resonance band center frequencies.

be clearly attributed to the presence of the second antenna. Moreover, the H-plane cross-pol far-field radiation pattern, shown in Figure 11(b), further highlights the importance of adding the ground strips, since sufficiently small values of cross-polarization can be only attained in this case, where the additional strips suppress parasitic, ground-induced cross polarization.

3.3. Opposite Sided MIMO CSRR Antennas

The exact same procedure, as in the previous section, was followed for the MIMO antenna configuration of Figure 4(c). In the case of the antenna with CLL element inclusion, shown in Figure 12(a), the simulated versus the experimental results are shown Figure 12(c). In this case, the MIMO antenna exhibits a first resonance at 2.456 GHz with a reflection coefficient of −12.93 dB. The first resonance band extends from 2.388 GHz to 2.491 GHz. The antenna at the resonance frequency exhibits a mutual coupling of −25.85 dB. Moreover, additional vertical thin strips were inserted in the antenna system of Figure 12(b), to suppress the flow of radiation between the ground conductors as in the previous case, with the direction of strips again being perpendicular to the direction of propagation. The simulated results for this particular case are shown in Figure 10(d). In this case, the antenna exhibits a resonance at 2.448 GHz with a minimum reflection coefficient of −22.67 dB. The mutual coupling between its radiating elements has been reduced to −45.12 dB at the resonance frequency. The experimental results reveal a center frequency of 2.447 GHz with a reflection coefficient of −22 dB and a mutual coupling of −26.9 dB. The graph of the envelope correlation coefficient is shown in Figure 9(b). Once again, this particular case of the MIMO antenna with the CLL resonator and the thin strips, exhibits the lowest near-zero ρ_e in the vicinity of 2.45 GHz, in comparison with the other cases. Finally, the H-plane co-pol far-field patterns for all the antennas in the second configuration at their resonance frequencies is depicted in Figure 11(c), indicating again that omnidirectional characteristics are preserved, with the occurrence of some variations due to the presence of the second antenna. The cross-pol H-plane pattern

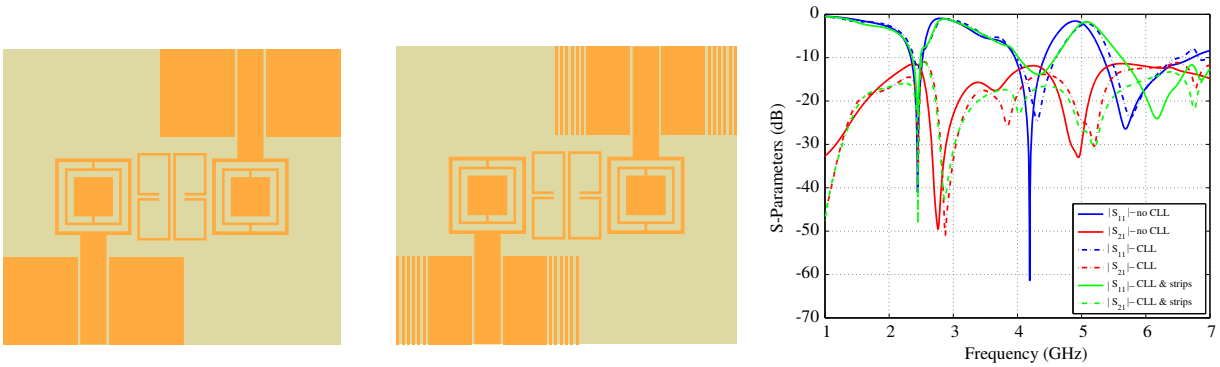

(a) (b) (c)

Figure 12. (a) MIMO antenna with CLL resonator. (b) MIMO antenna with CLL resonator and ground strips. (c) Simulated S-parameters versus frequency.

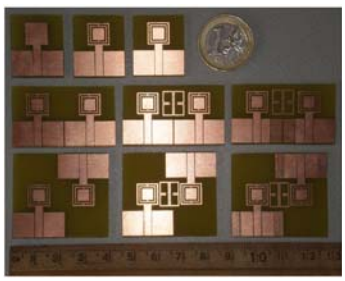

Figure 13. Fabricated set of antennas. First row depicts single monopole antennas. Second and third rows depict adjacent and opposite sided MIMO CSRR antennas, respectively.

of Figure 11(d), shows acceptable values of the cross-pol component in all cases, with an additional improvement being due to the presence of the ground strips in this case as well.

The final set of all fabricated antennas is depicted in Figure 13.

4. CONCLUSION

An electrically small metamaterial-inspired uniplanar antenna, based on the CSRR element, has been presented. Two different configurations of compact MIMO antennas have been implemented and metamaterial-inspired resonators have been used to reduce mutual coupling between closely spaced radiating elements. Whereas other designs have used similar methods for coupling isolation, most of the antennas used were either bulky $\lambda/4$ monopoles or complicated in structure. In addition, existing metamaterial-based designs are usually in three dimensional form, therefore, not practical. In contrast, the proposed technique retains its simplicity, ease of fabrication and compactness, since the CLL structure is subwavelength. Planarity is also fully maintained, since no metallic or other extrusions, vias or other 3D and high profile structures, are employed, as opposed to other metamaterial-inspired techniques. A particularly decisive advantage is that the design procedure and the parameter choice is highly systematic, since the CLL can be designed independently from the MIMO antenna, and no optimization or parametric design for the entire antenna is necessary, apart form minimal fine tuning. The overall approach is synthesized from antenna elements that are both small in size and closely spaced and is proven to be efficient, achieving both high isolation and satisfactory radiation efficiency.

ACKNOWLEDGMENT

This research was co-financed by the European Union (European Social Fund-ESF) and Greek national funds through the Operational Program "Education and Lifelong Learning" of the National Strategic Reference Framework (NSRF). Research Funding Program: THALES (Project ANEMOS), Investing in knowledge society through the European Social Fund.

REFERENCES

1. Pendry, J. B., A. J. Holden, W. J. Stewart, and I. Youngs, "Extremely low frequency plasmons in metallic mesostructures," *Phys. Rev. Lett.*, Vol. 76, No. 25, 4773–4776, 1996.
2. Pendry, J. B., A. J. Holden, D. J. Robbins, and W. J. Stewart, "Magnetism from conductors and enhanced nonlinear phenomena," *IEEE Trans. Microw. Theory Tech.*, Vol. 47, No. 11, 2075–2084, 1999.
3. Smith, D. R., W. J. Padilla, D. C. Vier, S. C. Nemat-Nasser, and S. Schultz, "Composite medium with simultaneously negative permeability and permittivity," *Phys. Rev. Lett.*, Vol. 84, No. 18, 4184–4187, 2000.
4. Smith, D. R., S. Schultz, P. Markoš, and C. M. Soukoulis, "Determination of effective permittivity and permeability of metamaterials from reflection and transmission coefficients," *Phys. Rev. B*, Vol. 65, 195104, 2002.
5. Smith, D. R., D. C. Vier, T. Koschny, and C. M. Soukoulis, "Electromagnetic parameter retrieval from inhomogeneous metamaterials," *Phys. Rev. E*, Vol. 71, 036617, 2005.
6. Li Hou, L., J. Y. Chin, X. M. Yang, X. Q. Lin, R. Liu, F. Y. Xu, and T. J. Cui, "Advanced parameter retrievals for metamaterial slabs using an inhomogeneous model," *J. Appl. Phys.*, Vol. 103, No. 6, 064904, 2008.
7. Qureshi, F., M. A. Antoniades, and G. V. Eleftheriades, "A compact and low-profile metamaterial ring antenna with vertical polarization," *IEEE Antennas Wireless Propag. Lett.*, Vol. 4, 333–336, 2005.
8. Alici, K. B. and E. Ozbay, "Electrically small split ring resonator antennas," *J. Appl. Phys.*, Vol. 101, No. 8, 083104, 2007.
9. Erentok, A. and R. W. Ziolkowski, "Metamaterial-inspired efficient electrically small antennas," *IEEE Trans. Antennas Propag.*, Vol. 56, No. 3, 691–707, 2008.

10. Huang, M. D. and S. Y. Tan, "Efficient electrically small prolate spheroidal antennas coated with a shell of double-negative metamaterials," *Progress In Electromagnetics Research*, Vol. 82, 241–255, 2008.
11. Zhu, J. and G. V. Eleftheriades, "Dual-band metamaterial-inspired small monopole antenna for WiFi applications," *Electron. Lett.*, Vol. 45, No. 22, 1104–1106, 2009.
12. Herraiz-Martínez, F. J., L. E. García-Muñoz, D. González-Ovejero, V. González-Posadas, and D. Segovia-Vargas, "Dual-frequency printed dipole loaded with split ring resonators," *IEEE Antennas Wireless Propag. Lett.*, Vol. 8, 137–140, 2009.
13. Antoniades, M. A. and G. V. Eleftheriades, "A broadband dual-mode monopole antenna using NRI-TL metamaterial loading," *IEEE Antennas Wireless Propag. Lett.*, Vol. 8, 258–261, 2009.
14. Zhu, J., M. A. Antoniades, and G. V. Eleftheriades, "A compact tri-band monopole antenna with single-cell metamaterial loading," *IEEE Trans. Antennas Propag.*, Vol. 58, No. 4, 1031–1038, 2010.
15. Ntaikos, D. K., N. K. Bourgis, and T. V. Yioultsis, "Metamaterial-based electrically small multiband planar monopole antennas," *IEEE Antennas Wireless Propag. Lett.*, Vol. 10, 963–966, 2011.
16. Ye, D., S. Xi, H. Chen, J. Huangfu, and L.-X. Ran, "Achieving large effective aperture antenna with small volume based on coordinate transformation," *Progress In Electromagnetics Research*, Vol. 111, 407–418, 2011.
17. Wang, P., G.-J. Wen, Y.-J. Huang, and Y.-H. Sun, "Compact CPW-fed planar monopole antenna with distinct triple bands for WiFi/WiMAX applications," *Electron. Lett.*, Vol. 48, No. 7, 357–359, 2012.
18. Li, K., C. Zhu, L. Li, Y.-M. Cai, and C.-H. Liang, "Design of electrically small metamaterial antenna with ELC and EBG loading," *IEEE Antennas Wireless Propag. Lett.*, Vol. 12, 678–681, 2013.
19. Falcone, F., T. Lopetegi, J. D. Baena, R. Marqués, F. Martín, and M. Sorolla, "Effective negative-ϵ stopband microstrip lines based on complementary split ring resonators," *IEEE Microw. Wireless Compon. Lett.*, Vol. 14, No. 6, 280–282, 2004.
20. Falcone, F., T. Lopetegi, M. A. G. Laso, J. D. Baena, J. Bonache, M. Beruete, R. Marqués, F. Martín, and M. Sorolla, "Babinet principle applied to the design of metasurfaces and metamaterials," *Phys. Rev. Lett.*, Vol. 93, No. 19, 197401, 2004.
21. Baena, J. D., J. Bonache, F. Martín, R. M. Sillero, F. Falcone, T. Lopetegi, M. A. G. Laso, J. García-García, I. Gil, M. F. Portillo, and M. Sorolla, "Equivalent-circuit models for split-ring resonators and complementary split-ring resonators coupled to planar transmission lines," *IEEE Trans. Microw. Theory Tech.*, Vol. 53, No. 4, 1451–1461, 2005.
22. Anguera, J., A. Andújar, M.-C. Huynh, C. Orlenius, C. Picher, and C. Puente, "Advances in antenna technology for wireless handheld devices," *International Journal of Antennas and Propagation*, Vol. 2013, Article ID 838364, 2013.
23. Foschini, G. J. and M. J. Gans, "On limits of wireless communications in a fading environment when using multiple antennas," *Wireless Personal Communications*, Vol. 6, No. 3, 311–335, 1998.
24. Vaughan, R. G. and J. B. Andersen, "Antenna diversity in mobile communications," *IEEE Trans. Veh. Technol.*, Vol. 36, No. 4, 149–172, 1987.
25. Abouda, A. A. and S. G. Häggman, "Effect of mutual coupling on capacity of MIMO wireless channels in high SNR scenario," *Progress In Electromagnetics Research*, Vol. 65, 27–40, 2006.
26. Farahani, H. S., M. Veysi, M. Kamyab, and A. Tadjani, "Mutual coupling reduction in patch antenna arrays using a UC-EBG superstrate," *IEEE Antennas Wireless Propag. Lett.*, Vol. 9, 57–59, 2010.
27. Coulombe, M., S. F. Koodiani, and C. Caloz, "Compact elongated mushroom (EM)-EBG structure for enhancement of patch antenna array performances," *IEEE Trans. Antennas Propag.*, Vol. 58, No. 4, 1076–1086, 2010.
28. Zhu, J. and G. V. Eleftheriades, "A simple approach for reducing mutual coupling in two closely spaced metamaterial-inspired monopole antennas," *IEEE Antennas Wireless Propag. Lett.*, Vol. 9,

379–382, 2010.

29. Han, X., H. Hafdallah-Ouslimani, T. Zhang, and A. C. Priou, "CSRRs for efficient reduction of the electromagnetic interferences and mutual coupling in microstrip circuits," *Progress In Electromagnetics Research B*, Vol. 42, 291–309, 2012.
30. Han, M. and J. Choi, "Multiband MIMO antenna using orthogonally polarized dipole elements for mobile communications," *Microw. Opt. Techn. Lett.*, Vol. 53, No. 9, 2043–2048, 2011.
31. Park, S. and C. Jung, "Compact MIMO antenna with high isolation performance," *Electron. Lett.*, Vol. 46, No. 6, 390–391, 2010.
32. Sarrazin, J., Y. Mahé, S. Avrillon, and S. Toutain, "Collocated microstrip antennas for MIMO systems with a low mutual coupling using mode confinement," *IEEE Trans. Antennas Propag.*, Vol. 58, No. 2, 589–592, 2010.
33. Ferrer, P. J., J. M. González-Arbesú, and J. Romeu, "Decorrelation of two closely spaced antennas with a metamaterial AMC surface," *Microw. Opt. Technol. Lett.*, Vol. 50, No. 5, 1414–1417, 2008.
34. Bait-Suwailam, M. M., M. S. Boybay, and O. M. Ramahi, "Electromagnetic coupling reduction in high-profile monopole antennas using single-negative magnetic metamaterials for MIMO applications," *IEEE Trans. Antennas Propag.*, Vol. 58, No. 9, 2894–2902, 2010.
35. Hsu, C.-C., K.-H. Lin and H.-L. Su, "Implementation of broadband isolator using metamaterial-inspired resonators and a T-shaped branch for MIMO antennas," *IEEE Trans. Antennas Propag.*, Vol. 59, No. 10, 3936–3939, 2011.
36. Sharawi, M S., A. B. Numan, and D. N. Aloi, "Isolation improvement in a dual-band dual-element MIMO antenna system using capacitively loaded loops," *Progress In Electromagnetics Research*, Vol. 134, 247–266, 2013.
37. Yaghjian, A. D. and S. R. Best, "Impedance, bandwidth, and Q of antennas," *IEEE Trans. Antennas Propag.*, Vol. 53, No. 4, 1298–1324, 2005.
38. Mavridis, G. A., D. E. Anagnostou, and M. T. Chryssomallis, "Evaluation of the quality factor, Q, of electrically small microstrip-patch antennas," *IEEE Antennas Propag. Mag.*, Vol. 53, No. 4, 216–224, 2011.
39. Yaghjian, A. D., M. Gustafsson, and B. L. G. Jonsson, "Minimum Q for lossy and lossless electrically small dipole antennas," *Progress In Electromagnetics Research*, Vol. 143, 641–673, 2013.
40. Hrabar, S., Z. Eres, and J. Bartolic, "Capacitively loaded loop as basic element of negative permeability meta-material," *Proc. Eur. Microw. Conf.*, 357–361, Milan, Italy, 2002.
41. Erentok, A., P. L. Luljak, and R. W. Ziolkowski, "Characterization of a volumetric metamaterial realization of an artificial magnetic conductor for antenna applications," *IEEE Trans. Antennas Propag.*, Vol. 53, No. 1, 160–172, 2005.
42. Guo, Y., G. Goussetis, A. P. Feresidis, and J. C. Vardaxoglou, "Efficient modeling of novel uniplanar left-handed metamaterials," *IEEE Trans. Microw. Theory Tech.*, Vol. 53, No. 4, 1462–1468, 2005.
43. Thaysen, J. and K. B. Jakobsen, "Envelope correlation in (N, N) MIMO antenna array from scattering parameters," *Microw. Opt. Technol. Lett.*, Vol. 48, No. 5, 832–834, 2006.
44. Karatzidis, D. I., T. V. Yioultsis, and E. E. Kriezis, "Fast analysis of photonic crystal structures with mixed-order prism macroelements," *J. Lightw. Technol.*, Vol. 26, No. 13, 2002–2009, 2008.
45. Aydin, K. and E. Ozbay, "Identifying magnetic response of split-ring resonators at microwave frequencies," *Opto-Electon. Rev.*, Vol. 14, No. 3, 193–199, 2006.
46. Wheeler, H. A., "Fundamental Limitations of small antennas," *Proc. IRE*, Vol. 35, No. 12, 1479–1484, 1947.
47. Ziolkowski, R. W. and A. Erentok, "At and below the chu limit: Passive and active broad bandwidth metamaterial-based electrically small antennas," *IET Microw. Antennas Propag.*, Vol. 1, No. 1, 116–128, 2007.
48. McLean, J. S., "A re-examination of the fundamental limits on the radiation Q of electrically small antennas," *IEEE Trans. Antennas Propag.*, Vol. 44, No. 5, 672–676, 1996.